Journal of Materials Chemistry A

Single ion conducting separator and dual mediators-based electrolyte for high-performance lithium-oxygen battery with non-carbon cathode

Journal:	*Journal of Materials Chemistry A*
Manuscript ID	TA-COM-03-2018-002567.R1
Article Type:	Communication
Date Submitted by the Author:	09-Apr-2018
Complete List of Authors:	Wu, Shichao; AIST, Qiao, Yu; AIST, Deng, Han; AIST Zhou, HaoShen; AIST,

Journal Name

COMMUNICATION

Single ion conducting separator and dual mediators-based electrolyte for high-performance lithium-oxygen battery with non-carbon cathode†

Received 00th January 20xx,
Accepted 00th January 20xx

DOI: 10.1039/x0xx00000x

www.rsc.org/

Shichao Wu,[#a] Yu Qiao,[#a] Han Deng,[a] and Haoshen Zhou*[ab]

The application of non-carbon cathodes for mitigating side reactions in lithium-oxygen batteries faces the critical disadvantages of significantly reduced discharge capacity and unsatisfying charge potential. Here, we break through these bottlenecks by introducing two synergistic redox mediators (RMs) into electrolyte for lithium peroxide formation and reversible oxidation, respectively, and more importantly, by developing a single ion conducting Li^+-Nafion separator to prohibit RMs crossover towards Li metal anode. The self-discharge and shuttle problems are avoided. The discharge capacity of the commercial ruthenium oxide-based non-carbon cathode can be greatly enhanced from 800 mAh g^{-1} to 3800 mAh g^{-1}. The charge potential can be significantly reduced to 3.2 V, which is among the best levels reported. During the long-term cycling, the battery keeps low charge overpotentials of 0.24 V, indicating high stability. This first synergistic concept of designing RMs and Li^+-Nafion separator for advanced non-carbon lithium-oxygen battery shows the great potential for developing practical batteries with high capacity, energy efficiency and rechargeability.

Introduction

Lithium-oxygen (Li-O_2) batteries have received lots of attention as potential next-generation energy storage medium due to their high energy density (~3500 Wh kg^{-1}).[1] A Li-O_2 battery is generally composed of a Li metal anode, a separator, an electrolyte and an air cathode. Their ideal work mechanism is based on the formation of lithium peroxide (Li_2O_2) during discharge process and its reversible decomposition during charge process (overall reaction: $2Li^+ + O_2 + 2e^- \rightleftharpoons Li_2O_2$, E^o = 2.96 V).[2–6] Although the processes seem simple, it was reported the discharge process involves several steps.[7,8] Firstly, O_2 is electrochemically reduced to superoxide (O_2^-) on air cathode ($O_2 + e^- \rightarrow O_2^-$). O_2^- species can either be absorbed on the surface of cathode or dissolve into the electrolyte. The absorbed O_2^- species are further electrochemically reduced to Li_2O_2 film covering on the surface of cathode ($O_2^- + 2Li^+ + e^- \rightarrow Li_2O_2$, surface-mediated reaction). Once the Li_2O_2 film grows to a thickness of several nanometers, the insulation nature of Li_2O_2 would cease the conduction of e^- and Li^+ and then result in the termination of electrochemical reactions and premature battery death.[9] On the other hand, the dissolved O_2^- species can chemically disproportionate into O_2 and Li_2O_2 ($2LiO_2 \rightarrow Li_2O_2 + O_2$, solution-mediated reaction). Li_2O_2 can evolve into large particles with several micrometers until all the voids in cathode are occupied. Whether the surface-mediated reaction or solution-mediated reaction dominates, it mainly depends on the properties of cathode materials and Gutmann number of electrolyte solvent, lithium salt and additive.[10] Generally, in electrolytes with low Donor number (DN) or Acceptor number (AN), the Li-O_2 batteries shows limited discharge capacity due to the undesired surface-mediated reaction route. In any case, the generation of O_2^- is inevitable.

In the presence of strongly oxidative O_2^- intermediator and Li_2O_2 products, the popularly-used carbon for air cathode was reported to suffer from serious decomposition.[11–14] The generated Li_2CO_3 byproducts passivate the cathode, resulting in the decreased electron/ion conductivity and poor catalysis activity.[15] In this case, Li-O_2 battery shows low discharge capacity, large discharge/charge overpotential and limited cycling stability.[16] In order to avoid the carbon corrosion, non-carbon materials as air cathode have been extensively explored.[17] Nanoporous Au,[18] Ru/ITO,[19] TiC,[20] nanostructured Ti_4O_7,[21] and metallic RuO_2 with morphologies of hollow sphere,[22] nanosheet,[23] and mesoporous hydrangea-like particle,[24] have been suggested as potential substitutes for carbon materials. However, the Li-O_2 batteries based on these non-carbon cathodes can only achieve low discharge capacity (<900 mAh g^{-1}) even after deliberate structure designs. This

[a] Energy Technology Research Institute, National Institute of Advanced Industrial Science and Technology (AIST), 1-1-1, Umezono, Tsukuba 305-8568, Japan. E-mail: hs.zhou@aist.go.jp
[b] Center of Energy Storage Materials & Technology, College of Engineering and Applied Sciences, National Laboratory of Solid State Microstructures, Collaborative Innovation Center of Advanced Microstructures, Nanjing University, Nanjing, 210093, China. E-mail: hszhou@nju.edu.cn
# These two authors contribute equally to this research.
† Electronic Supplementary Information (ESI) available. See DOI: 10.1039/x0xx00000x

significantly sacrifices the cardinal superiority (high energy density) of Li-O_2 battery. It is indispensable to improve the capacity of non-carbon-based Li-O_2 battery by a simple technique.

Recently, Bruce's group introduced an electrolyte additive 2,5-di-tert-butyl-1,4-benzoquinone (DBBQ) to suppress surface-mediated Li_2O_2 film formation and promote solution-mediated growth of Li_2O_2 particle.[25] During discharge, DBBQ is reduced to $DBBQ^-$ before O_2 reduction on cathode. The soluble $DBBQ^-$ chemically reacts with O_2 to produce Li_2O_2 and DBBQ. The battery capacity was greatly enhanced even for carbon cathode with low specific surface areas. Inspired by these results, we expected the capacity of non-carbon cathode could be effectively enhanced by introducing DBBQ additive in the electrolyte. At present, there are few studies on this combination.

Another problem is that, DBBQ, when contacting with Li metal anode, will inevitably be reduced and consumed. This is because DBBQ has a high reduction potential of ~2.75 V. The reaction between Li and DBBQ can be examined from the photo

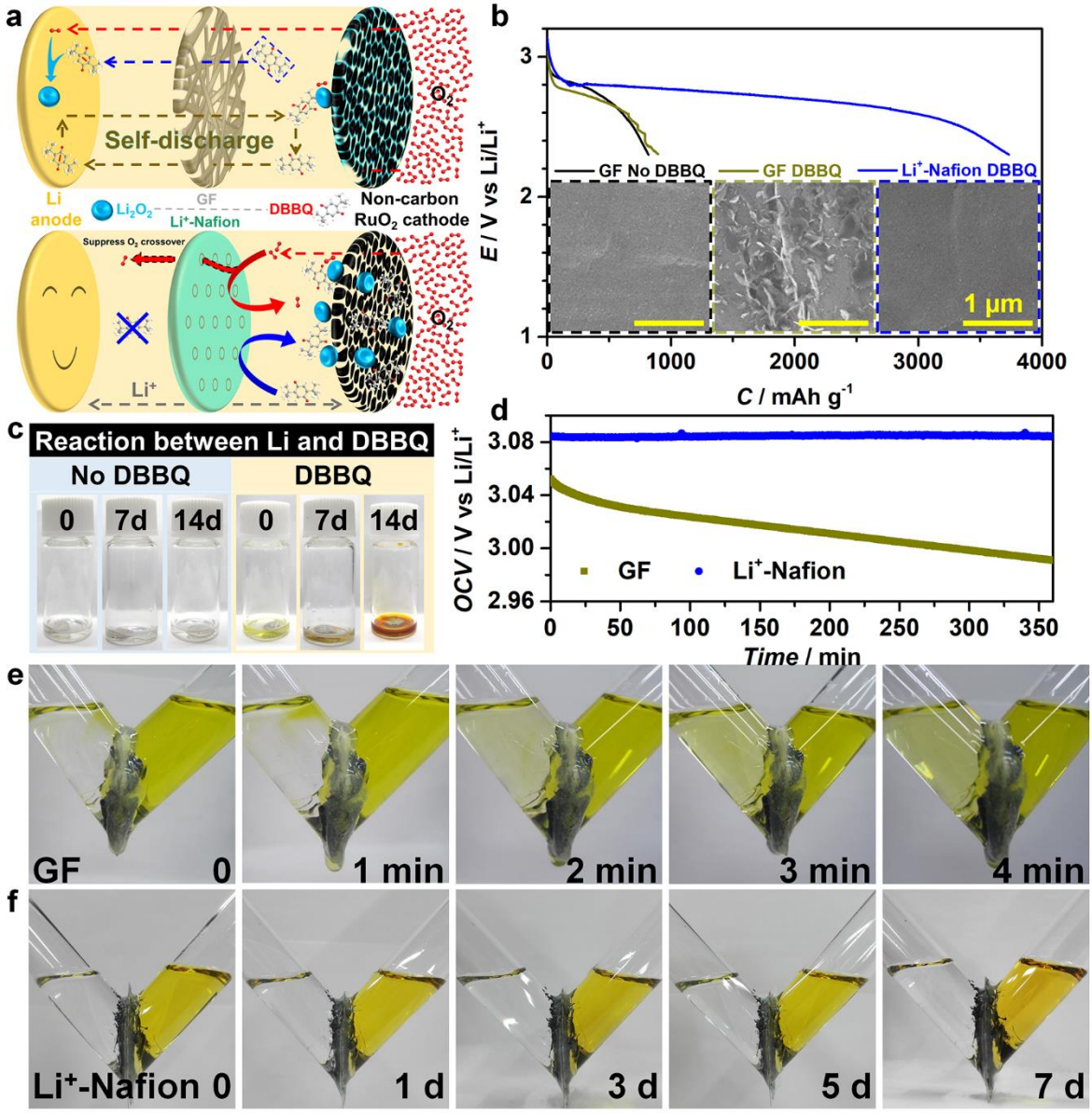

Figure 1. Block of DBBQ by Li^+-Nafion membrane and enhanced capacity of Li-O_2 battery with non-carbon RuO_2 cathode. (a) Schematic illustration of problems related to Li-O_2 battery with DBBQ in electrolyte and GF separator and schematic illustration of improvements of Li-O_2 battery with Li^+-Nafion membrane as separator. (b) Full discharge profiles of non-carbon RuO_2 cathode-based Li-O_2 batteries without DBBQ, with DBBQ and GF separator and with DBBQ and Li^+-Nafion separator, respectively Current density: 20 mA g^{-1}. Insets are the SEM images of Li metal anodes in discharged Li-O_2 batteries without DBBQ, with DBBQ and GF separator and with DBBQ and Li^+-Nafion separator, respectively. (c) Photos showing the color changes of the DBBQ-containing/free electrolytes for 14 days when immersing a piece of Li metal, respectively. (d) Open circuit voltage (OCV) evolution of non-carbon RuO_2 cathode-based Li-O_2 batteries with DBBQ-GF separator and with DBBQ-Li^+-Nafion separator, respectively. (e) Permeation experiment to observe the block effect of GF separator towards DBBQ in electrolyte. (f) Permeation experiment to observe the block effect of Li^+-Nafion membrane towards DBBQ in electrolyte.

in Figure 1c. After immersing Li metal into electrolyte with DBBQ for several days, the electrolyte color changed from light yellow to dark brown. In comparison with no color change for DBBQ-free electrolyte, the reaction between Li and DBBQ can be confirmed. Therefore, in the previous articles, the impractical $LiFePO_4$ electrode instead of Li metal was used as the counter electrode to study the function of DBBQ towards oxygen reduction reaction (ORR) on air cathode.[25] However, exploring available solution to prohibit DBBQ crossover has rarely been investigated.

Herein, we construct stable non-carbon commercial RuO_2 as air cathode, DBBQ as ORR redox mediator (RM) in electrolyte and single ion conducting Li^+-Nafion membrane as separator to fabricate Li-O_2 batteries. Non-carbon RuO_2 cathode permits the elimination of carbon-related side reactions; DBBQ in electrolyte efficiently overcomes the disadvantage (low capacity) of non-carbon cathode; Li^+-Nafion separator prohibits DBBQ crossover towards Li metal anode and the induced self-discharge problem. The synergistic technique allows Li-O_2 battery with non-carbon cathode achieves large capacity improvement from ~800 mAh g^{-1} to ~3800 mAh g^{-1}. After developing an effective RM for oxygen evolution reaction (OER) and solving the related shuttle effect by Li^+-Nafion separator, the battery shows ultralow charge potential (~3.2 V) and long-term cycling stability.

Results and discussions

The non-carbon cathodes were prepared by coating the mixture of commercial RuO_2 and Lithion binder on Al current collector. The particle sizes of RuO_2 range from 50 nm to 100 nm (SEM image in Figure S1). The specific surface area is 20 m^2 g^{-1}.[23] The pristine electrolyte is 1 M LiTFSI in tetraglyme (G4). The control separator is glass fiber (GF), which is commonly used for Li-O_2 batteries. Li metal is the anode. As shown in Figure 1b, in electrolyte without any RM, the RuO_2 cathode shows a low full discharge capacity of ~800 mAh g^{-1} at a current density of 20 mA g^{-1}. This value is far below the general capacity of common carbon cathode and it will significantly decrease the energy density of Li-O_2 battery. Aim to increase the capacity, DBBQ as the ORR RM was added into electrolyte. However, the discharge capacity only increased slightly to ~900 mAh g^{-1} when GF separator was used. As confirmed from the photos in Figure 1c, DBBQ can be reduced by Li metal anode. Considering the GF separator has large pore sizes, DBBQ can easily penetrate and diffuse to Li metal anode (Figure 1e). The block effect of commercial Celgard separator towards DBBQ was also poor (Figure S2). Meanwhile, O_2 gas goes through separator to Li metal anode. On Li metal anode, DBBQ reacts with Li to produce LiDBBQ which further reactions with O_2 to generate Li_2O_2 particles (Figure 1a). Partial LiDBBQ can diffuse back to cathode and result in the formation of Li_2O_2 on cathode during storage, causing self-discharge phenomenon. The open circuit voltage (OCV) ceaselessly decreased before discharge (Figure 1d). These chemical reactions can occur spontaneously without any connection between electrodes, decreasing the shelf life of Li-O_2 batteries and causing them to initially have less than a full capacity when actually putting to use. From the SEM image of Li metal anode in the discharged Li-O_2 battery with DBBQ-containing electrolyte and GF separator, large amounts of small Li_2O_2 particles depositing on the surface of Li metal anode can be observed. This is contrast with the smooth surface of Li metal anode when there was no DBBQ in electrolyte and the pristine Li metal anode (Figure S3). These results verified the fact that DBBQ and O_2 could pass through GF separator and there were reactions between DBBQ, O_2 and Li metal anode. In order to prohibit the DBBQ crossover, we adopted Li^+-Nafion membrane to substitute GF separator. The Li^+ ion conductivity in the Li^+-Nafion membrane-based cell is ~0.5 mS cm^{-1} (Figure S4), which is approaching the value of GF separator-based cell. From the permeation experiment in Figure 1f, it was confirmed that no DBBQ penetrated the Li^+-Nafion membrane for 7 days. Nafion

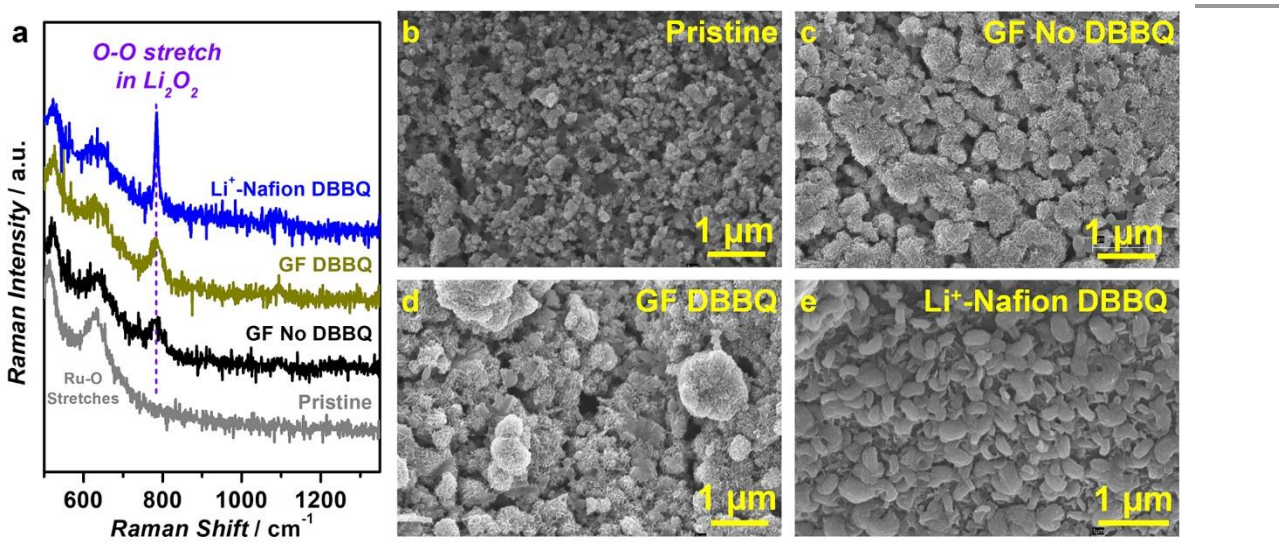

Figure 2. Characterization of discharge products on cathodes. (a) Raman spectra of pristine RuO_2 cathode, discharged RuO_2 cathode without DBBQ, discharged RuO_2 cathode with DBBQ and GF separator, discharged RuO_2 cathode with DBBQ and Li+-Nafion separator, respectively. SEM images of (b) pristine RuO_2 cathode, (c) discharged RuO_2 cathode without DBBQ, (d) discharged RuO_2 cathode with DBBQ and GF separator, (e) discharged RuO_2 cathode with DBBQ and Li^+-Nafion separator, respectively.

membrane with metal-ion exchange also was reported to show enhanced resistibility towards oxygen permeation.[26] Benefiting from efficient blocking effect of Li^+-Nafion membrane towards DBBQ (Figure 1a), undesired self-discharge phenomenon and side reaction on Li metal can be eliminated. This ensures that all the DBBQ can play the role of ORR RM for capacity enhancement on RuO_2 cathode. In this case, Li-O_2 battery with the non-carbon RuO_2 cathode, DBBQ-containing electrolyte and Li^+-Nafion separator achieved steady OCV evolution (Figure 1d) and large discharge capacity of ~3800 mAh g^{-1} (Figure 1b), which was three times higher than those batteries without DBBQ in electrolyte and with DBBQ and GF separator. The Li metal anode after discharge showed flat surface and no particles could be seen. These results indicate that Li^+-Nafion separator indeed restricts DBBQ access to Li metal anode, guarantees the capacity-enhanced function of DBBQ as a ORR RM on non-carbon RuO_2 cathode and protects Li metal anode from passivation by undesired byproducts.

Discharge products on cathodes were analyzed by Raman spectra, SEM and X-ray diffraction (XRD) analysis. The Raman spectra in Figure 2a show the obvious peaks at Raman shift of ~780 cm^{-1}, confirming Li_2O_2 is the primary discharge products despite different peak intensities in all non-carbon RuO_2 cathode-based Li-O_2 batteries without DBBQ, with DBBQ and GF separator, with DBBQ and Li^+-Nafion separator. SEM image in Figure 2c indicates the discharged cathode in Li-O_2 battery without DBBQ shows very small particles (several tens of nanometers) covering the surface of RuO_2 particles. This morphology is because the RuO_2 particles have low specific surface area and the G4-LiTFSI electrolyte has low DN. In this case, surface-mediated reaction dominated during discharge, resulting in the limited growth of Li_2O_2 products. When the passivation layer of Li_2O_2 increases to the critical thickness, no more Li_2O_2 can be generated due to the poor ion and electron conductivity of Li_2O_2 layer and the discharge capacity reaches the final value. It can be seen there remain lots of voids unoccupied within the cathode. In the Li-O_2 battery with DBBQ and GF separator (Figure 2d), the discharged RuO_2 cathode presents the similar morphology to the cathode of battery without DBBQ. This can be ascribed to the migration of DBBQ to Li metal anode from cathode side and its consumption on Li metal anode (Figure 1e and inset SEM image in Figure 1b). Therefore, the discharge process mainly follows the surface-mediated reaction and no obvious capacity improvement can be realized (Figure 1b). Many voids still remain within the cathode. In contrast, when the Li^+-Nafion membrane is used as the separator, plenty of toroid-like Li_2O_2 particles with diameter of ~300 nm occupies the whole cathode surface, leaving nearly no more voids within the cathode. The typical large toroid-like morphology indicates DBBQ plays the critical role of phase-transfer catalysis in weakly solvating G4-LiTFSI electrolyte and facilitates the solution-mediated growth of Li_2O_2 instead of

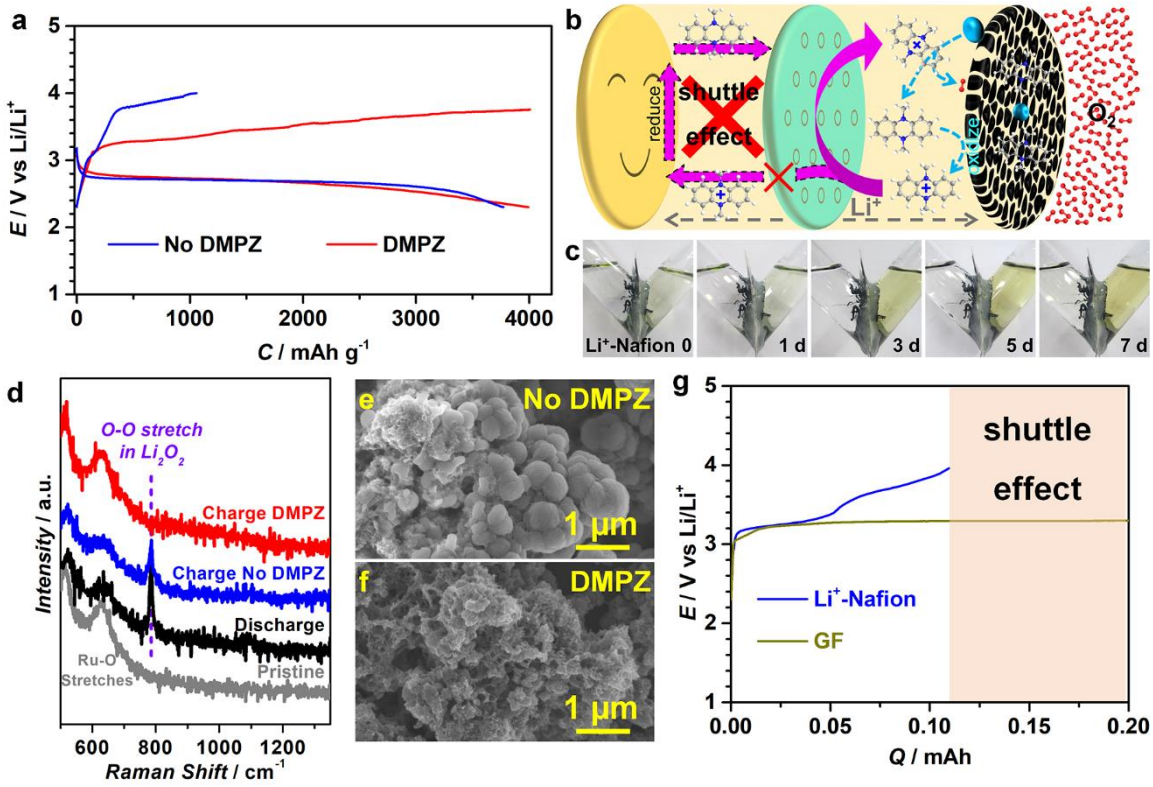

Figure 3. Improved charge performance of non-carbon RuO_2 cathode-based Li-O_2 battery with DBBQ in electrolyte and Li^+-Nafion separator by introducing DMPZ as OER RM. (a) Discharge-charge profiles of Li-O_2 batteries without DMPZ and with DMPZ. Current density: 20 mA g^{-1}. (b) Schematic illustration of the role of Li^+-Nafion separator for preventing DMPZ-induced shuttle effect during charge. (c) Permeation experiment to observe the block effect of Li^+-Nafion separator towards DMPZ in electrolyte. (d) Raman spectra of

charged RuO_2 cathodes in the absence/presence of DMPZ. SEM images of charged RuO_2 cathodes in the (e) absence/(f) presence of DMPZ, respectively. (g) Charge profile of Li-ion battery in Ar gas (RuO_2 cathode/separator infiltering DMPZ-containing electrolyte/Li anode) with GF separator and Li^+-Nafion separator, respectively.

surface-mediated growth. The XRD results in Figure S5 indicats the crystallization of the Li_2O_2 products in the presence of DBBQ is poor. These results underscore the importance of Li^+-Nafion separator for prohibiting DBBQ crossover and greatly enhancing capacity of non-carbon RuO_2 cathode-based Li-O_2 battery.

The synergistic integration of DBBQ in electrolyte and Li^+-Nafion separator ensures the capacity improvement of Li-O_2 battery with non-carbon RuO_2 cathode during discharge. The charge performance was further evaluated. As shown in Figure 3a, when the battery was recharged at 20 mA g^{-1}, high charge potential of > 3.8 V was observed and the terminal charge capacity was only ~1100 mAh g^{-1}, which was much less than the discharge capacity of 3800 mAh g^{-1}, indicating the low Coulombic efficiency. Raman spectra in Figure 3d suggest large amount of Li_2O_2 remains on the cathode. This can also be confirmed from the SEM image in Figure 3e. Undecomposed Li_2O_2 particles can be observed. The unsatisfactory charge ability is because the produced large Li_2O_2 particles during discharge have poor contact with the electrode surface and therefore Li_2O_2 is difficult to be electrochemically oxidized.[25] Employing liquid OER RMs to charge the Li-O_2 battery has been proved as a promising solution for improving battery charge performance.[27–30] Here, we used 5,10-dimethylphenazine (DMPZ) with a low charge potential (~3.2 V) as the OER RM.[31] After introducing DMPZ into electrolyte, it can be seen the charge potential is largely reduced to ~3.25 V and the terminal charge capacity can achieve the same value of discharge capacity, suggesting the high Coulombic efficiency. The Li_2O_2 peak in Raman spectra (Figure 3d) and Li_2O_2 particles in SEM image (Figure 3f) completely disappear, indicating the full oxidation of Li_2O_2 and the high reversibility of Li-O_2 battery. Another advantage of using Li^+-Nafion separator is that DMPZ cannot diffuse through Li^+-Nafion membrane (Figure 3c) and thus the DMPZ-induced shuttle effect can be prohibited (Figure 3b). In contrast, the GF and Celgard separators cannot prevent DMPZ penetration (Figure S5). When the GF separator was used in Li-ion battery with configuration of RuO_2 cathode/separator infiltering DMPZ-containing electrolyte/Li anode, the charge potential lasted at ~3.2 V (Figure 3g) and showed no increase even after the capacity exceeded the practical capacity (0.11 mAh that was confirmed in a LiSICON-based battery in Figure S6). This phenomenon is due to that partial oxidized DMPZ on cathode diffuses through GF separator to Li metal anode and is reduced to DMPZ, which can return to cathode and again form the oxidized DMPZ (Figure 3b). It likes the polysulfide-induced shuttle effect in Li-S battery.[32,33] In contrast, when the Li^+-Nafion separator was used, the profile exhibited the typical charge process. DMPZ could be oxidized at ~3.2 V and 3.75 V,[31] respectively and more importantly, the charge process terminated after the battery reached the practical value, indicating no shuttle effect. In Li-O_2 battery with Li^+-Nafion separator, the migration of oxidized DMPZ to Li metal anode and the reduction of the oxidized DMPZ by Li metal anode can be avoided. In this case, all the DMPZ can efficiently devotes its OER RM's role to decomposing Li_2O_2 and the Li-O_2 battery can realize the true reversibility.

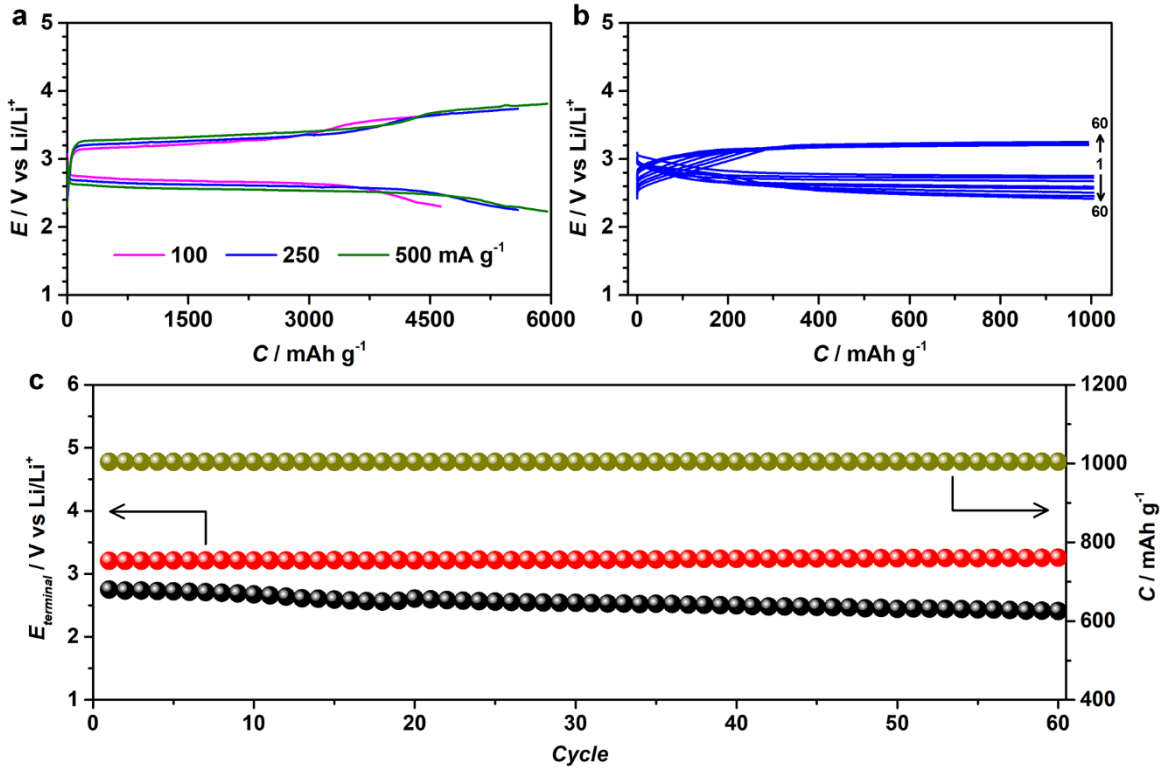

Figure 4. High rate capability and long-term cycling stability of non-carbon RuO_2-based Li-O_2 battery with DBBQ and DMPZ in electrolyte and Li^+-Nafion separator. (a) Discharge-charge profiles at 100, 250 and 500 mA g^{-1}. (b) Selected discharge-charge profiles during cycling at 250 mA g^{-1}. (c) Evolutions of discharge capacities and terminal discharge/charge potentials during cycling.

The rate capability of non-carbon RuO_2-based Li-O_2 battery with DBBQ and DMPZ in electrolyte and Li^+-Nafion separator was further evaluated at current densities of 100, 250 and 500 mA g^{-1}, respectively. As shown in Figure 4a, the discharge capacity, unexpectedly, increases from ~4600 mAh g^{-1} at 100 mA g^{-1}, to ~5200 mAh g^{-1} at 250 mA g^{-1} and ~5800 mAh g^{-1} at the large current density of 500 mA g^{-1}. This unique phenomenon is different from that in the carbon-based Li-O_2 battery with DBBQ in electrolyte (capacity decreases as current density increases).[25] It may be attributed to the elimination of cathode-related side reactions,[34] and needs further investigation. In all cases, the charge potentials hold at low value of ~3.2 V, corresponding to the overpotential of ~0.24 V, which is among the best levels reported. These results indicate the potential of applying this Li-O_2 battery system to provide high power density. In the long-term discharge-charge cycling at 250 mA g^{-1} (Figure 4b, c), the capacities show no decrease and more importantly, the charge potentials keep the very low values of ~3.2 V and the terminal potentials are well controlled below 3.4 V, indicating the stable cycling performance. At 500 mA g^{-1} and 2000 mAh g^{-1} (Figure S7), the battery can also keep low discharge/charge potential gaps (<0.6 V) for a long term. During cycling, the slightly increased overpotentials may due to the produced byproducts (Li_2CO_3, lithium formate and lithium acetate, etc.) from the inevitable decomposition of organic solvent (G4),[35] and this could be addressed by developing stable electrolyte solvents or employing highly-concentrated aqueous electrolyte.[36] After cycling, the absence of toroid-like Li_2O_2 particles on the cathode, the remaining light-yellow of the Li metal anode and the white color of the GF separator on the anode side confirmed the efficient block effect of Li^+-Nafion separator toward mediators in the actual environment inside the cell. The high rate capability and stable cycling performance suggest the critical role of the systematic integration of dual RMs (DBBQ and DMPZ) and the Li^+-Nafion separator that prohibits the RMs-induced self-discharge and shuttle effects (Figure 1 and 3).

Conclusions

In summary, the capacity of Li-O_2 battery based on the non-carbon commercial RuO_2 cathode was significantly improved from ~800 mAh g^{-1} to more than 3800 mAh g^{-1}. The charge potential was successfully reduced to an ultralow value of ~3.2 V along with the terminal potential below 3.6 V, which are among the best levels reported. High rate capability and long-term cycling stability were achieved. These enhancements were realized by developing DBBQ and DMPZ as ORR and OER redox mediators, respectively, and more importantly by originally proposing the use of Li^+-Nafion separator to prevent the self-discharge and shuttle problems resulting from the crossover of redox mediators towards Li metal anode. Although the electrolyte-absorbing ability and the ion conductivity of the Li^+-Nafion membrane should be further improved, this, to the best of our knowledge, is the first attempt to advance the performance of Li-O_2 battery through this systematic concept and should initiate more devotions on developing alternative solutions.

Conflicts of interest

There are no conflicts to declare.

Acknowledges

We are grateful for the partial financial support from the ALCA, Project of JST of Japan, the National Basic Research Program of China (2014CB932300) and NSF of China (21633003).

Notes and references

1 K. M. Abraham and Z. Jiang, *J. Electrochem. Soc.*, 1996, **143**, 1–5.
2 Z. Lyu, Y. Zhou, W. Dai, X. Cui, M. Lai, L. Wang, F. Huo, W. Huang, Z. Hu and W. Chen, *Chem. Soc. Rev.*, 2017, **46**, 6046–6072.
3 Z. Chang, J. Xu and X. Zhang, *Adv. Energy Mater.*, 2017, **7**, 1700875.
4 C. Yang, J. Han, P. Liu, C. Hou, G. Huang, T. Fujita, A. Hirata and M. Chen, *Adv. Mater.*, 2017, **29**, 1702752.
5 Z. Guo, D. Zhou, X. Dong, Z. Qiu, Y. Wang and Y. Xia, *Advanced Materials*, 2013, **25**, 5668–5672.
6 S. Wu, Y. Qiao, S. Yang, M. Ishida, P. He and H. Zhou, *Nature Communications*, 2017, **8**, 15607.
7 L. Johnson, C. Li, Z. Liu, Y. Chen, S. A. Freunberger, P. C. Ashok, B. B. Praveen, K. Dholakia, J.-M. Tarascon and P. G. Bruce, *Nat Chem*, 2014, **6**, 1091–1099.
8 H.-D. Lim, B. Lee, Y. Bae, H. Park, Y. Ko, H. Kim, J. Kim and K. Kang, *Chem. Soc. Rev.*, 2017, **46**, 2873–2888.
9 J. Wang, Y. Zhang, L. Guo, E. Wang and Z. Peng, *Angew. Chem. Int. Ed.*, 2016, **55**, 5201–5205.
10 N. B. Aetukuri, B. D. McCloskey, J. M. García, L. E. Krupp, V. Viswanathan and A. C. Luntz, *Nature Chemistry*, 2014, **7**, 50–56.
11 X. Zhang, L. Guo, L. Gan, Y. Zhang, J. Wang, L. R. Johnson, P. G. Bruce and Z. Peng, *J. Phys. Chem. Lett.*, 2017, **8**, 2334–2338.
12 M. M. Ottakam Thotiyl, S. A. Freunberger, Z. Peng and P. G. Bruce, *J. Am. Chem. Soc.*, 2013, **135**, 494–500.
13 D. M. Itkis, D. A. Semenenko, E. Y. Kataev, A. I. Belova, V. S. Neudachina, A. P. Sirotina, M. Hävecker, D. Teschner, A. Knop-Gericke, P. Dudin, A. Barinov, E. A. Goodilin, Y. Shao-Horn and L. V. Yashina, *Nano Lett.*, 2013, **13**, 4697–4701.
14 B. Zhou, L. Guo, Y. Zhang, J. Wang, L. Ma, W.-H. Zhang, Z. Fu and Z. Peng, *Adv. Mater.*, 2017, **29**, 1701568.
15 B. D. McCloskey, A. Speidel, R. Scheffler, D. C. Miller, V. Viswanathan, J. S. Hummelshøj, J. K. Nørskov and A. C. Luntz, *J. Phys. Chem. Lett.*, 2012, **3**, 997–1001.
16 S. Song, W. Xu, J. Zheng, L. Luo, M. H. Engelhard, M. E. Bowden, B. Liu, C.-M. Wang and J.-G. Zhang, *Nano Lett.*, 2017, **17**, 1417–1424.
17 I. Landa-Medrano, R. Pinedo, N. Ortiz-Vitoriano, I. R. de Larramendi and T. Rojo, *ChemSusChem*, 2015, **8**, 3932–3940.

18 Z. Peng, S. A. Freunberger, Y. Chen and P. G. Bruce, *Science*, 2012, **337**, 563–566.
19 F. Li, D.-M. Tang, Y. Chen, D. Golberg, H. Kitaura, T. Zhang, A. Yamada and H. Zhou, *Nano Lett.*, 2013, **13**, 4702–4707.
20 M. M. Ottakam Thotiyl, S. A. Freunberger, Z. Peng, Y. Chen, Z. Liu and P. G. Bruce, *Nature Materials*, 2013, **12**, 1050–1056.
21 D. Kundu, R. Black, E. J. Berg and L. F. Nazar, *Energy Environ. Sci.*, 2015, **8**, 1292–1298.
22 F. Li, D.-M. Tang, T. Zhang, K. Liao, P. He, D. Golberg, A. Yamada and H. Zhou, *Adv. Energy Mater.*, 2015, **5**, 1500294.
23 K. Liao, X. Wang, Y. Sun, D. Tang, M. Han, P. He, X. Jiang, T. Zhang and H. Zhou, *Energy Environ. Sci.*, 2015, **8**, 1992–1997.
24 C. Zhang, D. Tang, X. Hu, X. Liu, T. Zhang and H. Zhou, *Energy Storage Materials*, 2016, **2**, 8–13.
25 X. Gao, Y. Chen, L. Johnson and P. G. Bruce, *Nature Materials*, 2016, **15**, 882–888.
26 J. Qi, J. Ge, M. A. Uddin, Y. Zhai, U. Pasaogullari and J. St-Pierre, *Electrochimica Acta*, 2018, **259**, 510–516.
27 X. Gao, Y. Chen, L. R. Johnson, Z. P. Jovanov and P. G. Bruce, *Nature Energy*, 2017, **2**, 17118.
28 D. Kundu, R. Black, B. Adams and L. F. Nazar, *ACS Cent Sci*, 2015, **1**, 510–515.
29 W.-J. Kwak, D. Hirshberg, D. Sharon, M. Afri, A. A. Frimer, H.-G. Jung, D. Aurbach and Y.-K. Sun, *Energy & Environmental Science*, 2016, **9**, 2334–2345.
30 Z. Guo, C. Li, J. Liu, Y. Wang and Y. Xia, *Angew. Chem. Int. Ed.*, 2017, **56**, 7505–7509.
31 H.-D. Lim, B. Lee, Y. Zheng, J. Hong, J. Kim, H. Gwon, Y. Ko, M. Lee, K. Cho and K. Kang, *Nature Energy*, 2016, **1**, 16066.
32 S. Bai, X. Liu, K. Zhu, S. Wu and H. Zhou, *Nature Energy*, 2016, **1**, 16094.
33 R. Fang, S. Zhao, Z. Sun, D.-W. Wang, H.-M. Cheng and F. Li, *Adv. Mater.*, 2017, 1606823.
34 L. Lutz, W. Dachraoui, A. Demortière, L. R. Johnson, P. G. Bruce, A. Grimaud and J.-M. Tarascon, *Nano Lett.*, 2018, **12**, 1280–1289.
35 S. A. Freunberger, Y. Chen, N. E. Drewett, L. J. Hardwick, F. Bardé and P. G. Bruce, *Angew. Chem. Int. Ed.*, 2011, **50**, 8609–8613.
36 S. Wu, Y. Qiao, S. Yang, J. Tang, P. He and H. Zhou, *ACS Catal.*, 2018, **8**, 1082–1089.